Electronic Supporting Information

General: all reagents were purchased from commercial sources and used without further purification. Column chromatography was performed with silica gel 60 (Merck 9385, 230–400 mesh) or aluminium oxide 90 (neutral, act. II–III, Merck 1097).

NMR experimental : NMR spectra were acquired on a Bruker Avance-300 apparatus operating at 300.33 MHz for ^{1}H and 75.52 MHz for ^{13}C, equipped with a standard 4 mm H/X probe, with rotor spinning at 10 kHz. ^{1}H MAS spectra were acquired with 8 scans and 10 s as repetition delay. ^{13}C CPMAS acquisitions lasted 12 hours on average and involved a contact time equal to 2.5 ms, 5 s as repetition delay, 53 kHz and 63 kHz as ^{1}H and ^{13}C RF frequencies respectively and spinal64 composite pulse decoupling with 90 kHz ^{1}H RF frequency. A Bruker Avance-300 spectrometer was used for solution NMR analysis.

TGA and DSC experimental: TGA and DSC measurements were performed respectively on a Pyris 6 TGA (PerkinElmer) and a Jade DSC (PerkinElmer) apparatus .

Mass spectra were obtained with a VG-BIOQ triple quadrupole in positive mode (ES-MS).

Microanalyses were performed by the Service de Microanalyses de la Fédération de Recherche de Chimie, Université de Strasbourg, Strasbourg.

Data were collected at 173(2) K on a Bruker APEX8 CCD Diffractometer equipped with an Oxford Cryosystem liquid N_2 device, using graphite-monochromated Mo K (λ= 0.71073) radiation. The structures were solved using SHELXS-97 and refined by full matrix least-squares on F2 using SHELXL-97.21 The hydrogen atoms were introduced at calculated positions and not refined (riding model).

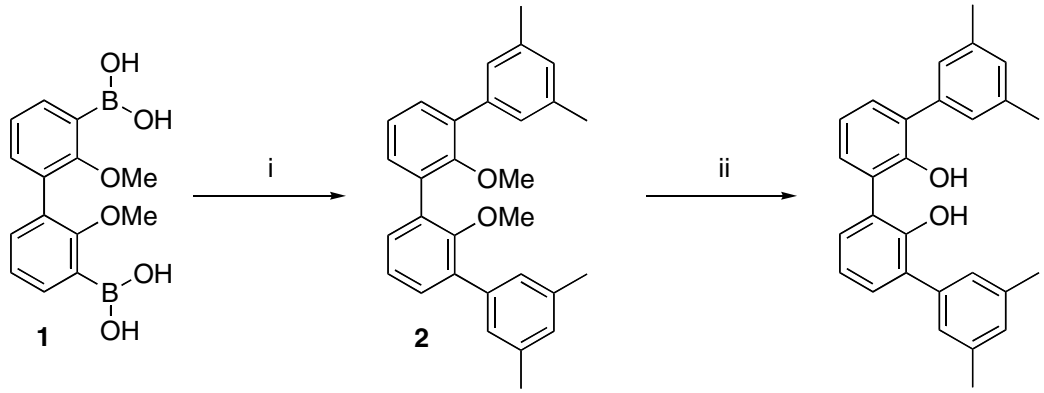

Figure 1: Synthetic pathway leading to the **http** derivative. i) $Pd(PPh_3)_4$, 5-bromo-*m*-xylene, Na_2CO_3, toluene / methanol / water, 80 °C, overnight, 55 %. ii) BBr_3, dichloromethane, 0 °C to room temperature, 85 %.

2',2''-dimethoxy-3,3''',5,5'''-tetramethyl-1,1':3',1'':3'',1'''-tetraphenyl (**2):**

The reaction was conducted under nitrogen. An aqueous Na_2CO_3 solution (10 mL 1 M) was transferred via canula to toluene (10 mL) containing 5-bromo-*m*-xylene (2.74 g, 14 mmol) and tetrakis(triphenylphosphine)palladium (50 mg, 0.043 mmol). After addition of a MeOH

solution (10 mL) of 2,2'-dimethoxy-1,1'-biphenyl-3,3'-bisboronic acid[(1)] (0.75 g, 2.48 mmol), the mixture was heated for 24 hours at 80°C, and tetrakis(triphenylphosphine)palladium (50 mg, 0.043 mmol) and 5-bromo-*m*-xylene (1.37 g, 7 mmol) were further added. After three days, the reaction was stopped, cooled to room temperature and some CH_2Cl_2 was added. The organic layer was isolated, dried ($MgSO_4$) and concentrated under reduced pressure. The residual solid was purified by chromatography (silica, pentane / CH_2Cl_2 70 : 30) to afford a white solid (0.585 g, 55 %). ^{1}H-NMR (300 MHz, $CDCl_3$): δ 7.34 (d, J = 7.5 Hz, 4H), 7.24-7.17 (complex, 6H), 6.99 (s, 2H), 3.28 (s, 6H), 2.37 (s, 12H). ^{13}C-NMR (75 MHz, $CDCl_3$): δ 155.2 (C), 138.8 (C), 137.5 (C), 135.3 (C), 132.8 (C), 130.7 (CH), 130.6 (CH), 128.7 (CH), 127.0 (CH), 123.4 (CH), 21.4 (CH_3). Mp 110 °C. MS (ES) : m/z 445.212 [calcd [M+Na]+ for $C_{30}H_{30}NaO_2$ 445.214]

(1) A. Kayal, A.F. Ducruet and S.C Lee *Inorg. Chem.* 2000, **39**, 3696.

2',2''-hydroxy-3,3''',5,5'''-tetramethyl-1,1':3',1'':3'',1'''-tetraphenyl (**http):**

The reaction was conducted under nitrogen. Compound **2** (585 mg, 13.86 mmol) was dissolved in freshly distilled dichloromethane (20 mL). To this solution was added dropwise at 0°C boron tribromide, 1M solution in methylene chloride (3.3 mL, 33 mmol). The resulting mixture was stirred overnight at room temperature and some water was carefully added. The organic layer was isolated, dried ($MgSO_4$) and concentrated under reduced pressure. The crude material was next purified over silica gel chromatography (pentane / CH_2Cl_2 70 : 30) leading to a white solid (469 mg, 85 %). ^{13}C-NMR (300 MHz, $CDCl_3$): δ 7.32 (d, J = 8.1 Hz, 4H), 7.16 (s, 4H), 7.10 (t, J = 7.5 Hz, 4H), 7.03 (s, 2H), 5.91 (s, 2H), 2.37 (s, 12H). ^{13}H-NMR (75 MHz, $CDCl_3$): δ 149.6 (C), 138.5 (C), 137,3 (C), 130.9 (CH), 130.3 (CH), 129.6 (C), 129.4 (CH), 127.1 (CH), 125.2 (C), 121.2 (CH), 21.3 (CH_3). Mp 155 °C. MS (ES) : m/z 417.183 [calcd [M+Na]+ for C28H26NaO2 417.183]

Crystals (**Phase I**) were obtained at 4°C by slow diffusion of pentane in a CH_2Cl_2 solution of **http**. X-ray data for **http**: Empirical formula $C_{28}H_{26}O_2$; Formula weight = 394.49 ; Crystal system : Orthorhombic ; Space group Pna2(1); Unit cell dimensions at T = 173(2) K: a = 7.4449(10) Å, b = 15.105(2) Å, c = 23.962(4) ; Volume = 2694.7(7) Å^3 ; Z = 4 ; Crystal size 0.20 x 0.20 x 0.18 mm^3 ; Theta range for data collection 2.70 to 27.50° ; Reflections collected 15980 ; Independent reflections 6078 [R(int) = 0.0542] ; Refinement method Full-matrix least-squares on F2 ; Data / restraints / parameters (6078 / 1 / 277) ; Goodness-of-fit on F2 :

1.018 ; Final R indices [I>2sigma(I)] R1 = 0.0892, wR2 = 0.2369 ; R indices (all data) R1 = 0.1330, wR2 = 0.2683 ; Extinction coefficient 0.30(2). CCDC 817017.

Crystals (**Phase II**) were obtained in a non-reproducible way by slow diffusion of hexane in a CH_2Cl_2 solution of **http**. X-ray data for **http** (**Phase II**): Empirical formula C_{28} H_{26} O_2 ; Formula weight = 394.49 ; Crystal system : Monoclinic ; Space group P2(1)/n ; Unit cell dimensions at T = 173(2) K: a = 7.9028(12) Å, b = 18.958(2) Å, c = 28.683(5), β = 91.060(3)° ; Volume = 4296.5(11) $Å^3$; Z = 8 ; Density 1220 $kg \cdot m^{-3}$; Crystal size 0.10 x 0.05 x 0.05 mm^3 ; Theta range for data collection 2.26 to 27.49° ; Reflections collected 30618 ; Independent reflections 9829 [R(int) = 0.0524] ; Refinement method Full-matrix least-squares on F2 ; Data / restraints / parameters (9829 / 0 / 554) ; Goodness-of-fit on F2 : 1.006 ; Final R indices [I>2sigma(I)] R1 = 0.0544, wR2 = 0.1297 ; R indices (all data) R1 = 0.1240, wR2 = 0.1606 ; Extinction coefficient 0.0050(6). CCDC 817018. Studies are in progress to find reproducible crystallisation conditions for **Phase II**.

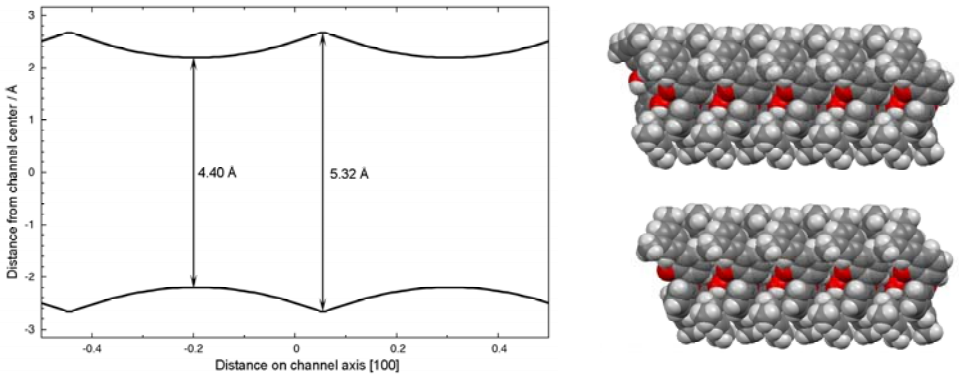

Figure 2: Channel aperture along the [100] axis assuming van der Waals radii of 1.2; 1.52 and 1.7 Å for H, O and C-atoms. View along the a-axis of the channel cross-section (spacefill model, Mercury software).

Thermal synthesis of **Phase II**: **Phase I** was converted to **Phase II** by heating the sample at 120 °C for a 20 minutes period.

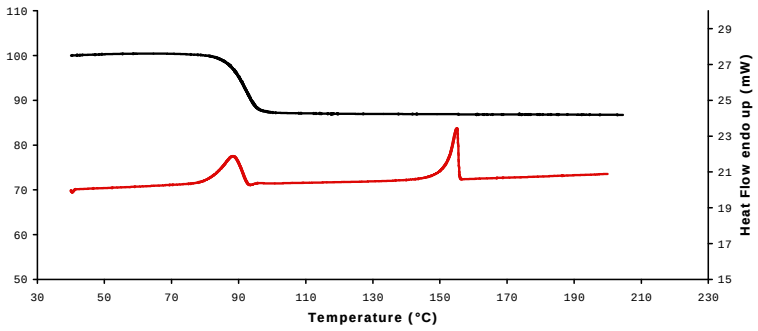

Figure 3: ATG (black curve) and DSC (red curve) traces for the **http** porous phase (**Phase I**) at 2 °C / min. It was checked that changing the heating rate has no significant effect on the DSC trace.

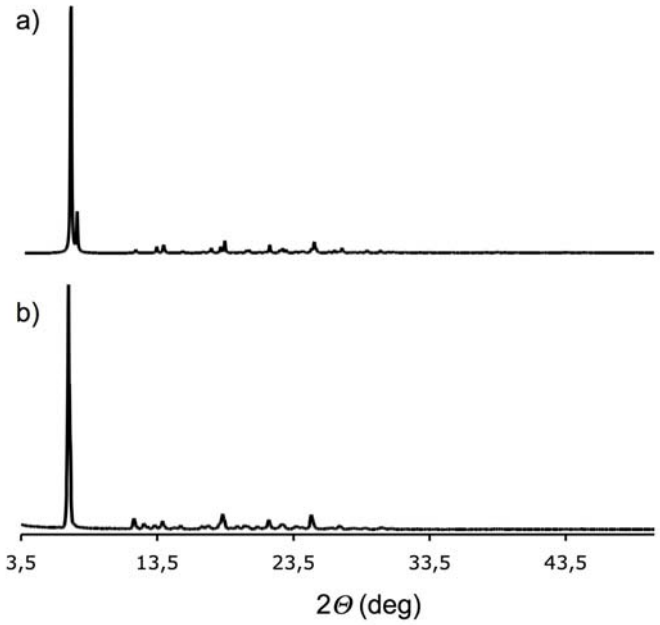

Figure 4: Simulated (a) and experimental (b) X-Ray powder diffractograms recorded for **http Phase I**. The diffractogram (a) has been simulated from X-Ray single crystal diffraction data obtained for **http** (**Phase I**).

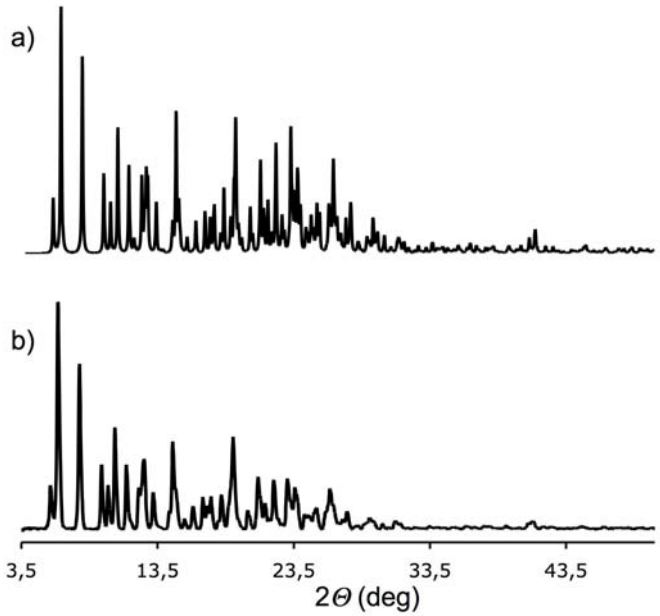

Figure 5: Simulated (a) and experimental (b) X-Ray powder diffractograms recorded for thermally synthesized **http Phase II**. **Phase I** was obtained at room temperature by slow diffusion of pentane in a CH_2Cl_2 solution of **http** and was heated over a period of 20 minutes at 120°C. The diffractogram (a) has been simulated from X-Ray single crystal diffraction data obtained for **http** (**Phase II**).

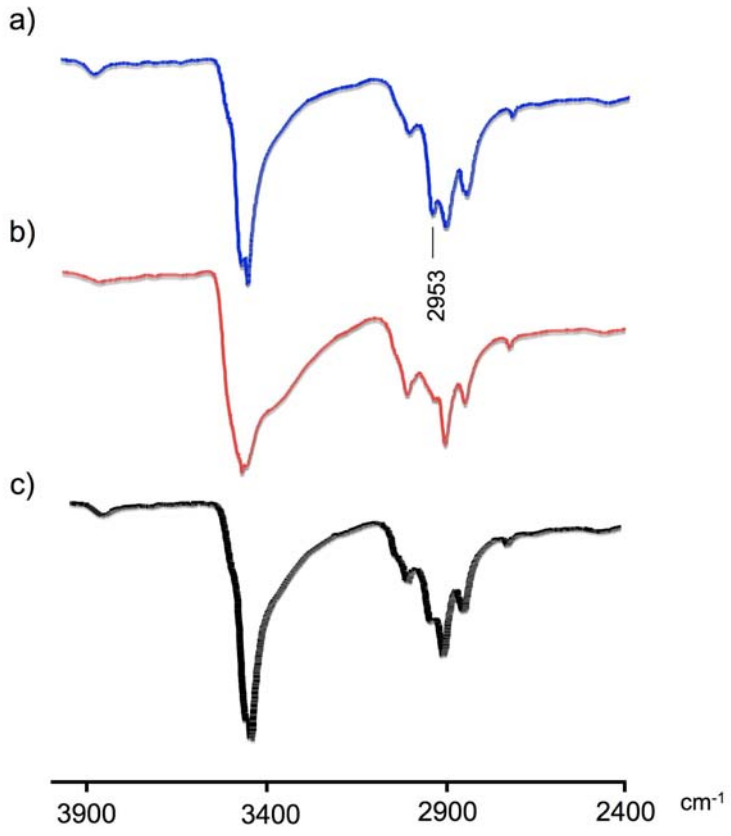

Figure 6: FTIR spectra of a) **Phase I**, b) the thermally synthesized **Phase II** and c) the resolvated **Phase I** obtained by exposing **Phase II** to an atmosphere saturated with dichloromethane and *n*-pentane vapours (50 / 50) for a 20 hours period.

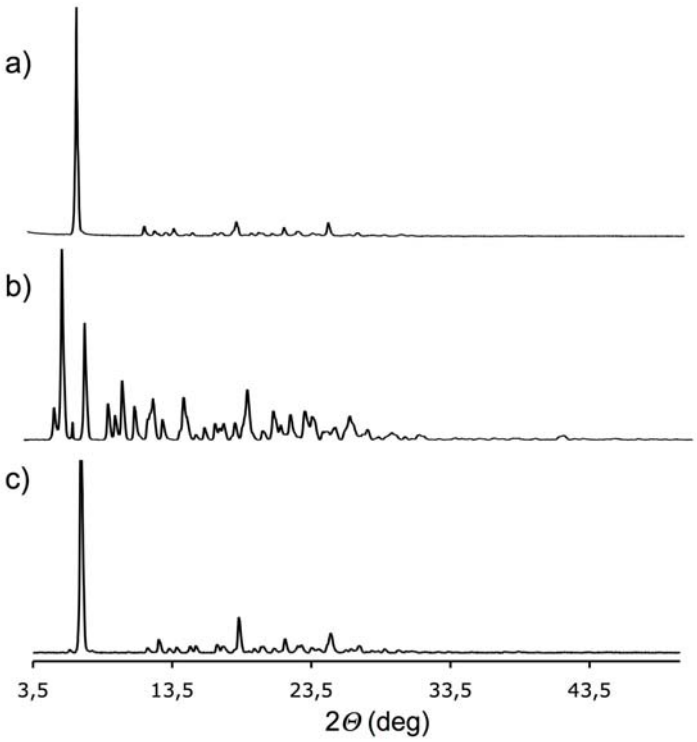

Figure 7a: A series of three diffractograms corresponding respectively to **Phase I** (a), the thermally synthesized **Phase II** obtained from **Phase I** (b) and the resolvated **Phase I** obtained by exposing **Phase II** to an atmosphere saturated with dichloromethane and *n*-pentane vapours (50 / 50) for a 11 hours period (c).

Phase II

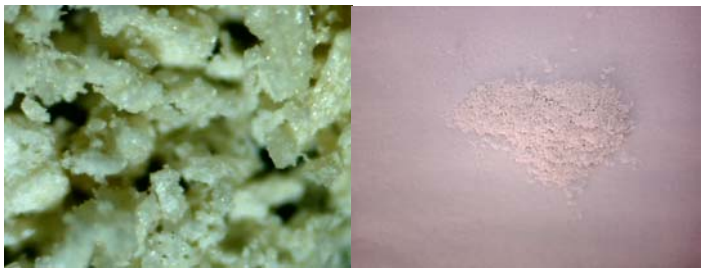

Phase I

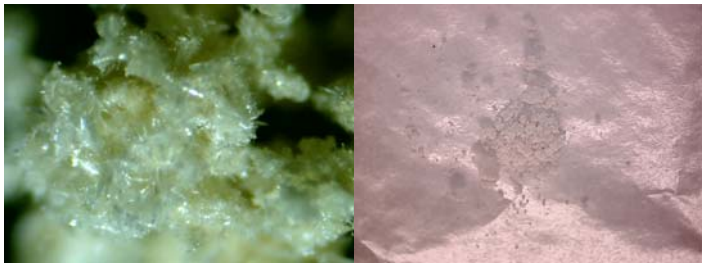

Figure 7b: Pictures of the crystalline powders corresponding to a thermally synthesized **Phase II** (two pictures at the top of this series) and to the resolvated **Phase I** obtained from the **Phase II** powder shown here.

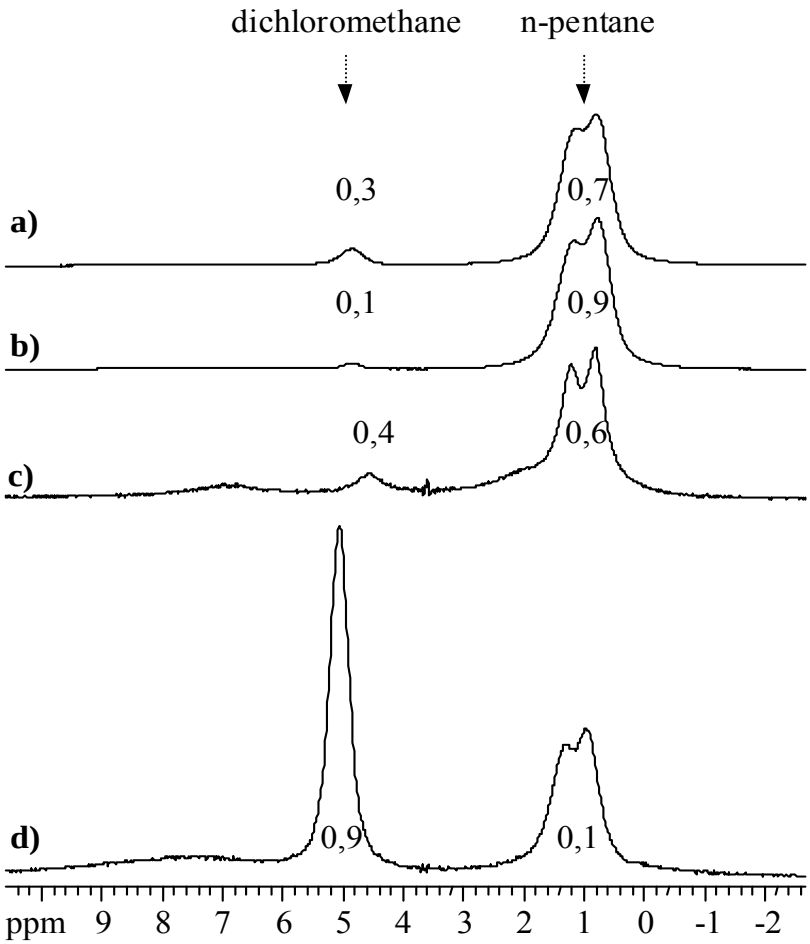

Figure 8: ^{1}H 10 kHz MAS spectra of **http** microcrystalline powder **a)** as-synthesized by diffusion of n-pentane into CH_2Cl_2 solution (**Phase I**), **b)** after further 20 days storage in air, **c)** after one night in oven at 100 °C (which gives **Phase II**, no solvent signals, spectrum not shown) and further exposure to CH_2Cl_2/*n*-pentane vapours during 2 h : first steps of re-solvation and **d)** same as **c)**, but after 36 hours contact with solvent vapors (re-solvation process ended, according to ^{13}C CPMAS spectrum shown in main text, figure 3). Relative molar fraction is mentioned for each solvent, determined by fitting with Dmfit software.(2) Note : spectra were corrected for probe signal and are displayed in a relative mode, with identical intensity for the highest pentane peak. Absolute intensities could not be compared here as the total quantity of analysed powder varied from one measurement to another. Only solvent proportions are significant.

(2) D. Massiot, F. Fayon, M. Capron, I. King, S. Le Calvé, B. Alonso, J.O. Durand, B. Bujoli, Z. Gan, G. Hoatson, *Magn. Reson. Chem.* 2002, **40**, 70.

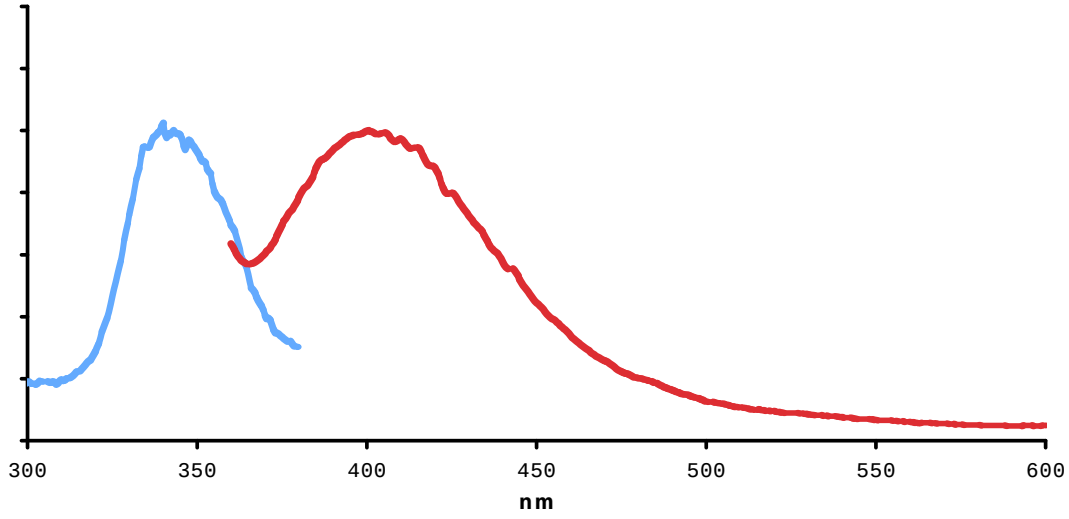

Figure 9: Excitation (blue line) (λ_{em} = 400 nm) and emission (red line) solid state fluorescence spectra for **http** (**Phase I**) (λ_{ex} = 340 nm). Note : The emission solid state fluorescence spectra for the compact structure (**Phase II**) is identical to the one obtained for **http** (**Phase I**) (represented here).

PACHA analysis

All calculations were made using the homemade PACHA software [1, 2]. The PACHA formalism relies on a unique partition of the total energy E_{tot} of an assembly of atoms into a self-energy SE-term modeling the electromagnetic coupling of the electrons and of the protons with the vacuum and a F-term modeling the electromagnetic coupling of the electrons and the protons with themselves:

$$E_{tot} = SE + F \qquad (1)$$

The key point is that for a given set of atomic coordinates, the dominant contribution to the long-range SE-term comes from the purely electrostatic interactions between electrons and nuclei that could be straightforwardly evaluated provided that equilibrium partial charges ($q = Z - N$, with Z number of protons in a given nucleus and N average number of electrons around this nucleus) are known. The quantum-mechanical F-term that encapsulates electron-electron correlations is on the other hand of very short range relative to the SE-term and is dominated by covalent bonding between atoms. Now, if two sub-systems A and B are brought into contact without breaking any covalent bonds, the initial spherical symmetry of the vacuum is broken leading to a large variation of the SE-term, whereas the quantum-mechanical F-term remains approximately the same. Applying the partition scheme (1) to each separated fragment leads to total energies $E_A = SE_A + F_A$ and $E_B = S_{EB} + F_B$. Provided that the two fragments are described by exactly the same set of atomic coordinates as the whole molecule (no structural relaxation), one may expect that:

$$F \approx F_A + F_B \quad \Rightarrow \quad E_{int} = E_{tot} - (E_A + E_B) \approx SE - (SE_A + SE_B) \qquad (2)$$

On this ground, the evaluation of interaction energies becomes straightforward and is perfectly suited for weak interactions that do not lead to large overlaps between electronic clouds such as van der Waals or hydrogen bonding. In all cases, the change in self-energies with distance, i.e. the shape (or structure) of the object governs the magnitude of the observed interaction and there is no need to perform a full quantum-mechanical treatment to recover reliable interaction energies. Obviously, this approach is doomed to fail if covalent bonds are created or broken during the approach of the two sub-systems, and in this case a full quantum-mechanical treatment becomes mandatory. Another case of failure is encountered when purely apolar systems interact leading to a very small SE-term that is now dominated by very short-range London-type or quadrupole-quadrupole interactions. From a practical point of view, a software was designed for retrieving reliable partial charges distributions from the sole knowledge of molecular or crystalline structure. Briefly stated, these charges are

recovered after application of the electronegativity equalization principle that is known to have a firm quantum-mechanical basis and a deep thermodynamic significance as a measure of the electronic chemical potential. The transformation of a set of atomic coordinates into a partial charges distribution is performed using an atomic parameterization resting on two non-empirical parameters per atom: an electronic chemical potential measured by a spectroscopic electronegativity (Allen's scale) and an atomic radius measured by the most diffuse principal maxima in the radial distribution function $r^2\psi^2(r)$, computed using relativistic wavefunctions solutions of the Dirac equations. One of the big advantages of the method is that it may be applied without any further modification either to molecular species or to crystalline networks. Concerning networks, it is worth noting that all computed charge distributions are fully converged owing to the systematic use of lattice sums techniques. This ensures that artefacts associated to truncation in the 1/r series are completely avoided, allowing fruitful comparisons between different crystal structures. Interested readers should refer to the original papers for more details [1, 2] and to other papers by our group for applications of this method to various situations [3-29]. After computation of a partial charges distribution from a given structural input (atomic coordinates describing a whole crystal structure or a molecular fragment derived from it), the corresponding SE-term is evaluated. Comparing the sum of SE-terms for two isolated sub-systems to the SE-term characterizing the two interacting systems allows getting characteristic interaction energies. In the following, we have applied such methods to the crystal structures described in the paper by giving for each fragment (crystalline or molecular), its characteristic SE-value. Moreover, in order to get interaction energies comparable to those derived from single-crystal neutron diffraction studies where distances involving H-atoms are much more reliably determined, all bonds involving H-atoms were scaled to a same averaged value (97 pm for O-H bonds and 108 pm for C-H)

Phase I

The whole network containing 4 **http** molecules per unit-cell was found to have SE(net) = -1319.7 $kJ.mol^{-1}$ to be compared with SE(http) = -307.1 $kJ.mol^{-1}$ for an isolated molecule, leading to a global interaction energy: E_{int} = (4x307.1 – 1319.7)/4 = -22.8 $kJ.mol^{-1}$. This value is to be associated to one O1-H…O2 intermolecular hydrogen bond responsible for the formation a 1D-chain and to the van der Waals stacking of such chains to form the 3D-network. In order to quantify the relative importance of networking interactions, charge distributions have been computed for a http dimer and for each sub-group of the $Pna2_1$ space-group. The self-energy of an isolated http H-bonded dimer was found to be SE(dim) = -634.6

kJ.mol^{-1} leading to an interaction energy: E_{dim}(HB) = (2x307.1 – 634.6)/2 = -10.2 kJ.mol^{-1}. On the other hand, selecting the Pa sub-group leads to isolated H-bonded http chains, a situation characterized by SE(Pa) = -657.9 kJ.mol^{-1} leading to an interaction energy: E_{chain}(HB) = (2x307.1 – 657.9)/2 = -21.9 kJ.mol^{-1}. Consequently a large cooperative effect is observed as the H-bond energy per http molecule is more than doubled on going from the gas phase to the solid-state. From this last value, the global stacking energy of the chains into a 3D-network is evaluated as: E_{stack}(3D) = 21.9 – 22.8 = -0.9 kJ.mol^{-1}, a rather small value typical of van der Waals interactions. This value should be compared to the value derived from SE(Pn) = -621.0 kJ.mol^{-1} characterizing a 1D-stacking of non H-bonded http molecules (Pn sub-group) and leading to E_{stack}(1D, Pn) = (2x307.1 – 621.0)/2 = -3.4 kJ.mol^{-1}. Similarly from SE($P2_1$) = -619.3 kJ.mol^{-1} characterizing a 3D-stacking of non H-bonded http molecules (Pn sub-group) one gets E_{stack}(3D, $P2_1$) = (2x307.1 – 619.3)/2 = -2.6 kJ.mol^{-1}. This shows clearly that the main cooperative networking interaction is the H-bonding between http molecules, against a moderately anti-cooperative (21.9 + 3.4 + 2.6 – 22.8 = +5.1 kJ.mol^{-1}) van der Waals stacking.

It is worth noticing that H-atoms positions of hydroxyl groups H1 and H2A have not been located from diffraction data but rather calculated from molecular geometry during the crystal structure refinement. As correctly pointed out by one referee of the MS, atom H2A is not engaged into H-bonding, a quite unusual situation. To clarify this point and check if there is not a more stable alternative, a self-energy and steric energy profile was computed for atoms H1 and H2A by rotating the O-H bonds by 360° along the O-C bond at constant H1-O1-C10 bond angle (109.5°). Figure 10 shows that H1-atom is trapped in an electrostatic energy well having a depth of about -172 kJ·mol^{-1} associated to a steric energy hill having a negligible height of about +2 kJ·mol^{-1}. Figure 11 shows that H2A-atom is also trapped in an electrostatic energy well having a depth of –162 kJ·mol^{-1} associated to a very flat steric energy well having a negligible depth of about +3 kJ·mol^{-1}. This analysis clearly shows that both H-atoms are trapped within wells having about the same depth, despite the fact that one H-atom (H1) is H-bonded to O2 and the other H-atom (H2A) is not H-bonded but rather engaged into a O-H…pi interaction with the aromatic ring made of atoms C15-C16-C17-C18-C19-C20. As both interactions are of the same order of magnitude from an electrostatic energy viewpoint the lack of H-bonding for H2A is not so surprising. To conclude, we have also optimized both torsion angles simultaneously leading to new atomic coordinates for H1 and H2A.

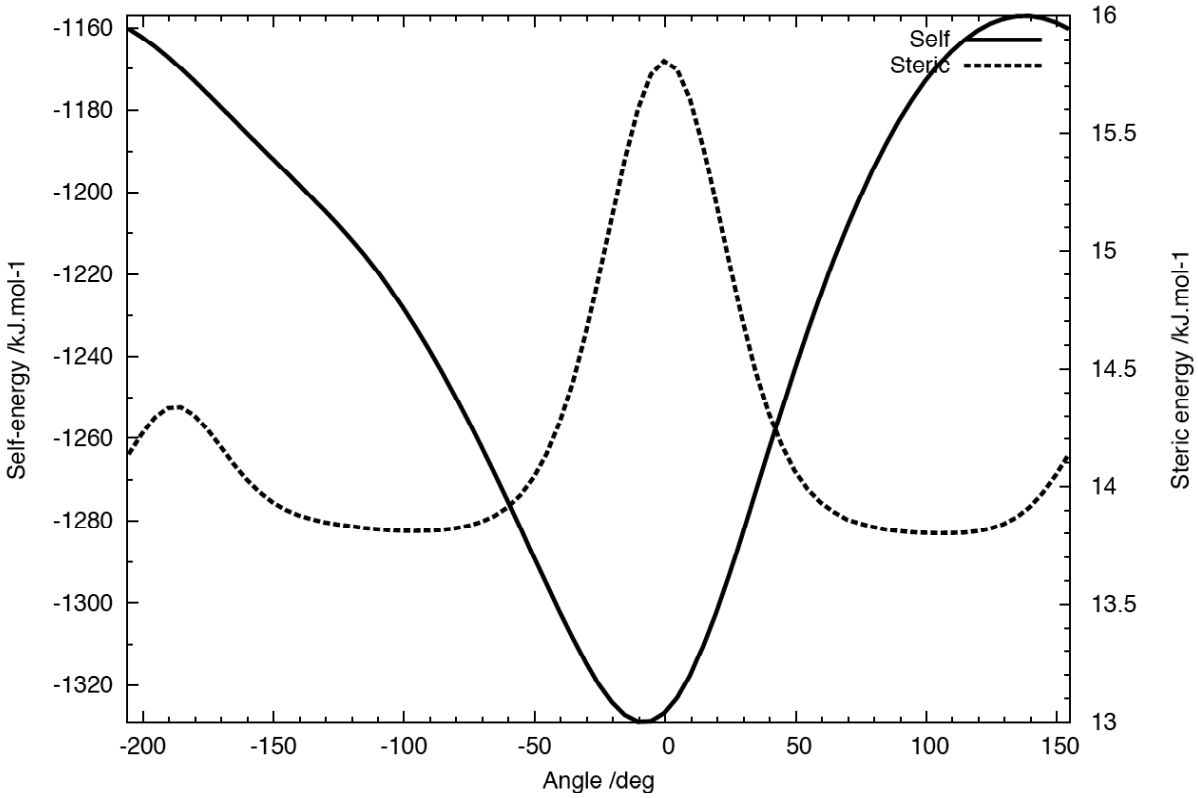

Figure 10: Energy profile obtained by rotating the O1-H1 bond by 360° along the O1-C10 bond at constant H1-O1-C10 bond angle (109.5°).

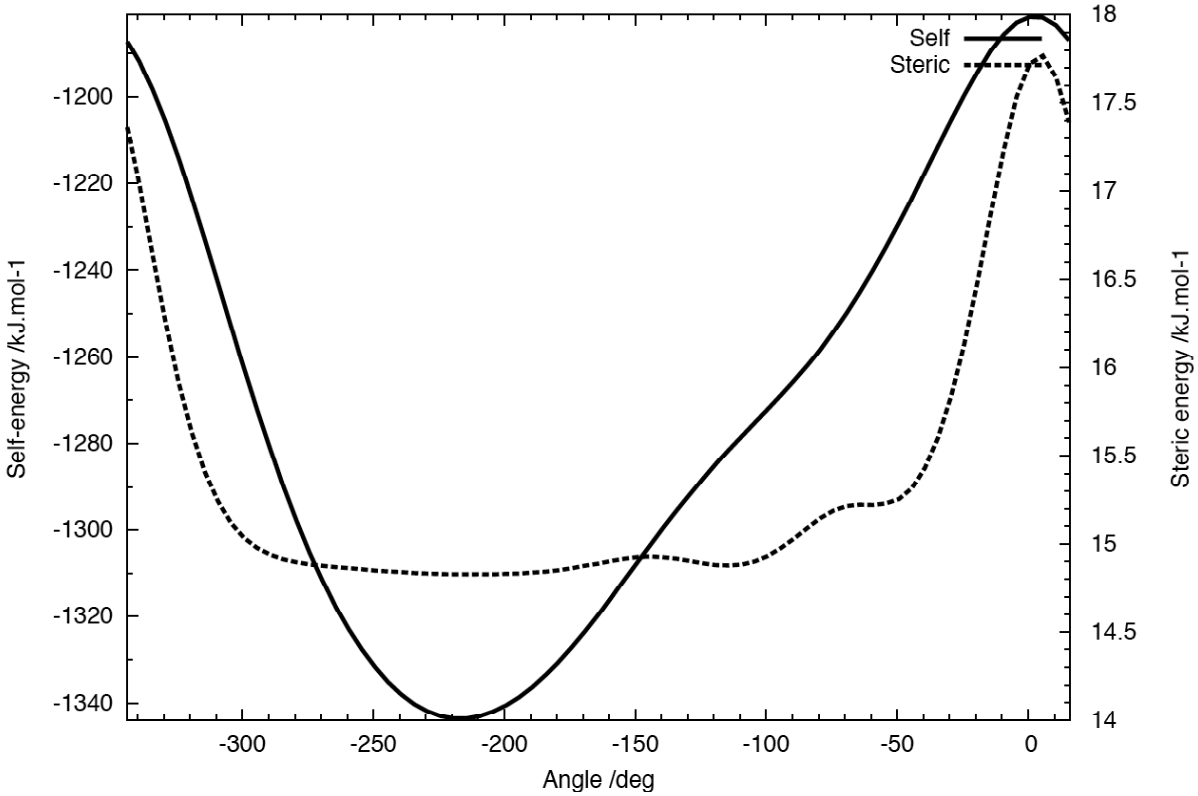

Figure 11: Energy profile obtained by rotating the O2-H2A bond by 360° along the O2-C16 bond at constant H2A-O2-C16 bond angle (109.5°).

After optimization, it was observed that the lattice energy decreased from -1319.7 kJ.mol^{-1} down to -1350.3 kJ.mol^{-1}, corresponding to an overall stabilization –31 kJ.mol^{-1}. Atomic coordinate for H1 was found to be (-0.0226, 0.17122, 0.38048) to be compared with XRD initial coordinates that were (-0.02949, 0.18002, 0.38718). This small change corresponds to a widening of O1-H1…O2(#3) bond angle from 143° in the XRD data up to 157° in the optimized data and to a shortening of the H1…O2(#3) bond length from 217 pm for the XRD data down to 208 pm in the optimized data. Similarly, optimized coordinates for H2A were found to be (0.42914, 0.31535, 0.27767) to be compared with XRD initial coordinates that were (0.33624, 0.33466, 0.28071). This significant shift in position corresponds to an overall shortening of all O-H…C distances of the aromatic ring pi-bonded to the hydroxyl moiety:

Pair	Distance XRD data /pm	Distance optimized data /pm
H2A…C15	336	280
H2A…C16	342	269
H2A…C17	324	255
H2A…C18	302	254
H2A…C19	294	265
H2A…C20	312	277

Apart from these small metrical changes, the overall topology is thus conserved and the small differences observed may be attributed to the fact that the XRD data refer to a situation where disordered solvent molecules are present even if they are not detected whereas the optimized data refer to a lattice with empty channels. In the solvent position optimization it was thus decided to keep the XRD metrics.

Phase II

The whole network containing 8 **http** molecules per unit-cell was found to have SE(net) = -2658.4 kJ.mol^{-1} to be compared with SE(**http1**) = -327.7 kJ.mol^{-1} and SE(**http2**) = -309.0 kJ.mol^{-1} for the two crystallographically non-equivalent isolated molecules, leading to a global interaction energy: E_{int} = (4x327.7 + 4x309.0 – 2658.4)/8 = -111.6/8 = -14.0 kJ.mol^{-1}. This overall destabilization relative to **Phase I** is obviously due to the fact that H-bonding networking interactions are limited to **http2** molecules, **http1** molecules being engaged in normal van der Waals stacking. In order to investigate the relative packing energies, a first sub-net was considered by discarding **http2** molecules, leading to SE_{net}(**http1**) = -1309.4 kJ.mol^{-1}. The average interaction energy within this sub-net is then: E_{int} = (4x327.7 – 1309.4)/4 = +1.4/4 = +0.4 kJ.mol^{-1}. This clearly shows that **http1** molecules are virtually not

involved into networking interactions and should thus be considered as merely filling the gaps generated by the removal of **http2** molecules. In order to further check this point the four possible sub-groups: $P2_1$, P-1 and Pn were investigated. The self-energy associated to the $P2_1$ stacking of **http1** molecules was found to be: SE_{net}(**http1**,$P2_1$) = -654.0 kJ.mol^{-1}, leading to an average interaction energy: E_{int} = (2x327.7 – 654.0)/2 = +1.4/2 = +0.7 kJ.mol^{-1}. Figure 12 shows that this sub-net is made of **http1** dimers at a distance of 230 pm associated into a 2D-layer at a longer distance of 260 pm. There is no stabilizing energy associated to this kind of stacking.

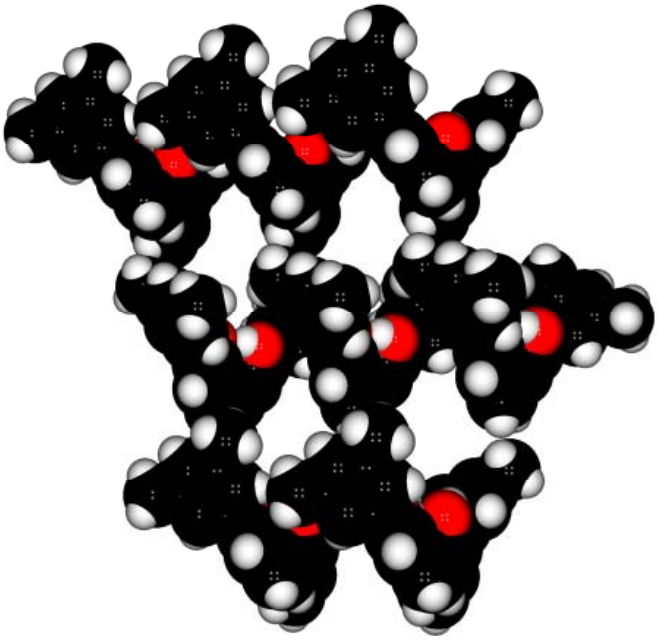

Figure 12: A 2D-layer of **http1** molecules stacked according to $P2_1$ space-group symmetry.

The self-energy associated to the P-1 stacking of **http1** molecules was found to be: SE_{net}(**http1**,P-1) = -654.9 kJ.mol^{-1}, leading to an average interaction energy: E_{int} = (2x327.7 – 654.9)/2 = +0.5/2 = +0.25 kJ.mol^{-1}. Figure 13 shows that this sub-net is made of chains of **http1** molecules at a distance of 230 pm associated into a 2D-layer at a longer distance of 260 pm. As before, there is no stabilizing energy associated to this kind of stacking.

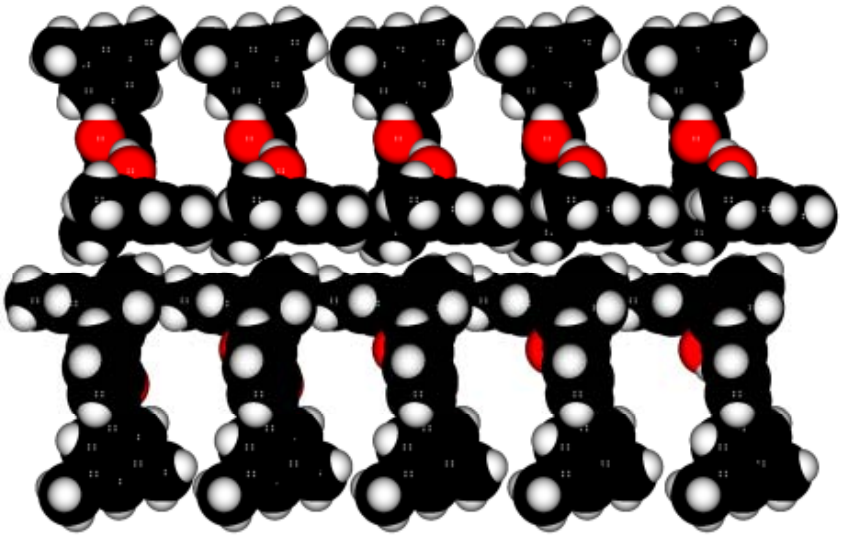

Figure 13: A 2D-layer of **http1** molecules stacked according to P-1 space-group symmetry.

The self-energy associated to the Pn stacking of **http1** molecules was found to be: SE_{net}(**http1**,Pn) = -653.5 kJ.mol^{-1}, leading to an average interaction energy: E_{int} = (2x327.7 – 653.5)/2 = +1.9/2 = +0.95 kJ.mol^{-1}. Figure 14 shows that this sub-net is made of chains of **http1** molecules at a distance of 230 pm associated into a 2D-layer at a longer distance of 260 pm. Again, there is no stabilizing energy associated to this kind of stacking.

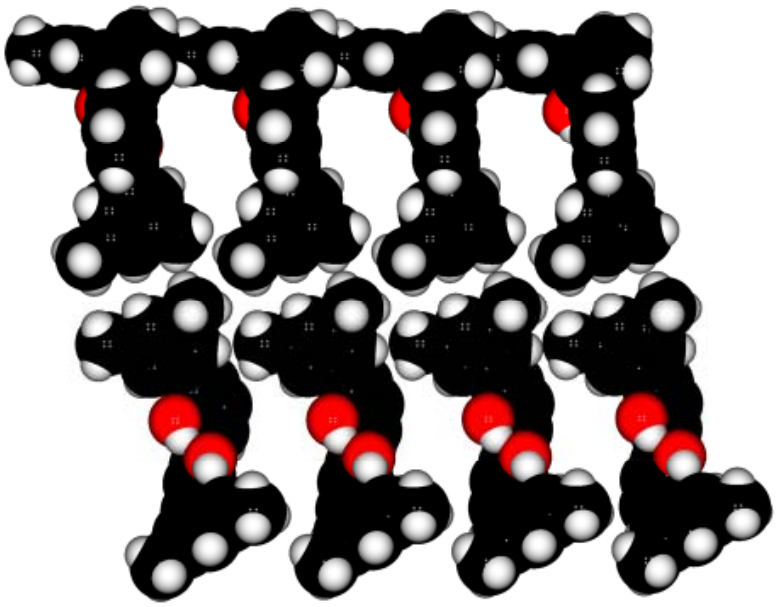

Figure 14: A 2D-layer of **http1** molecules stacked according to Pn space-group symmetry.

It follows from the preceding analysis that owing to their intra-molecular H-bonding interaction **http1** molecules are definitively not able to build a network alone as there is no

gain in energy between free isolated molecules and molecules stacked according to $P2_1/n$ space-group symmetry. The average destabilization energy for the three isolated sub-nets ($P2_1$, P-1 and Pn) was +0.6 kJ.mol^{-1}, a value that should be compared to the +0.4 kJ.mol^{-1} value characterizing the three interacting sub-groups $P2_1/n$. This shows that there is a very small cooperative effect (0.6 – 0.4 = –0.2 kJ.mol^{-1}) among **http1** molecules typical of van der Waals stacking.

A second sub-net was then considered by discarding **http1** molecules, leading to SE_{net}(**http2**) = -1257.2 kJ.mol^{-1}. The average interaction energy within this sub-net is then : E_{int} = (4x309.0 – 1257.2)/4 = -21.2/4 = -5.3 kJ.mol^{-1}. This confirms that **http2** molecules may be involved into networking interactions through favourable van der Waals stacking. In order to further check this point the four possible sub-groups: $P2_1$, P-1 and Pn were investigated. The self-energy associated to the $P2_1$ stacking of **http2** molecules was found to be: SE_{net}(**http2**,$P2_1$) = -625.5 kJ.mol^{-1}, leading to an average interaction energy: E_{int} = (2x309 – 625.5)/2 = -7.5/2 = -3.75 kJ.mol^{-1}. Figure 15 shows that this sub-net is made of layers of **http2** molecules at a distance of 260 pm. There is a small stabilizing energy associated to this kind of stacking.

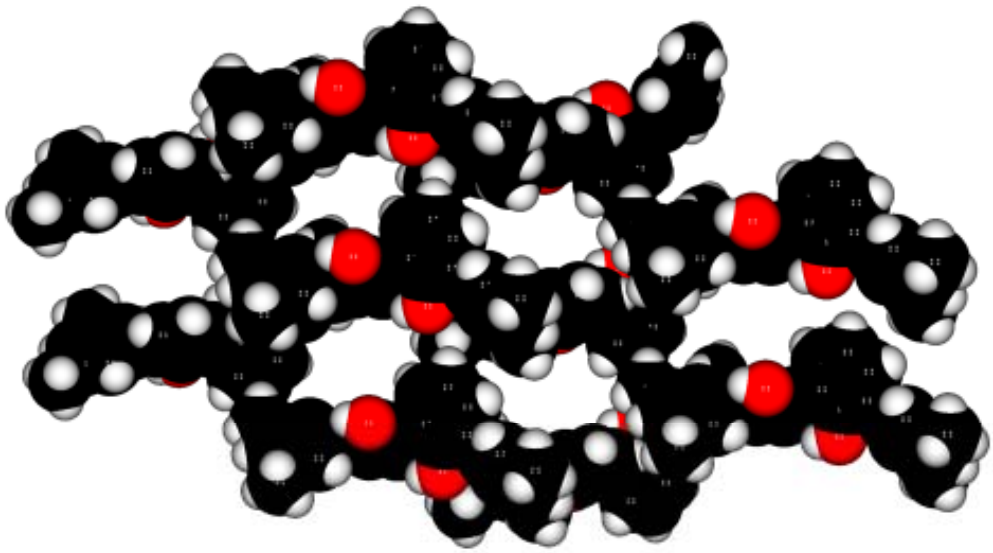

Figure 15: A 2D-layer of **http2** molecules stacked according to $P2_1$ space-group symmetry.

The self-energy associated to the P-1 stacking of **http2** molecules was found to be: SE_{net}(**http2**,P-1) = -624.5 kJ.mol^{-1}, leading to an average interaction energy: E_{int} = (2x309 – 624.5)/2 = -6.5/2 = -3.25 kJ.mol^{-1}. Figure 16 shows that this sub-net is made of layers of

http2 molecules at a distance of 230 pm. As before, there is a small stabilizing energy associated to this kind of stacking.

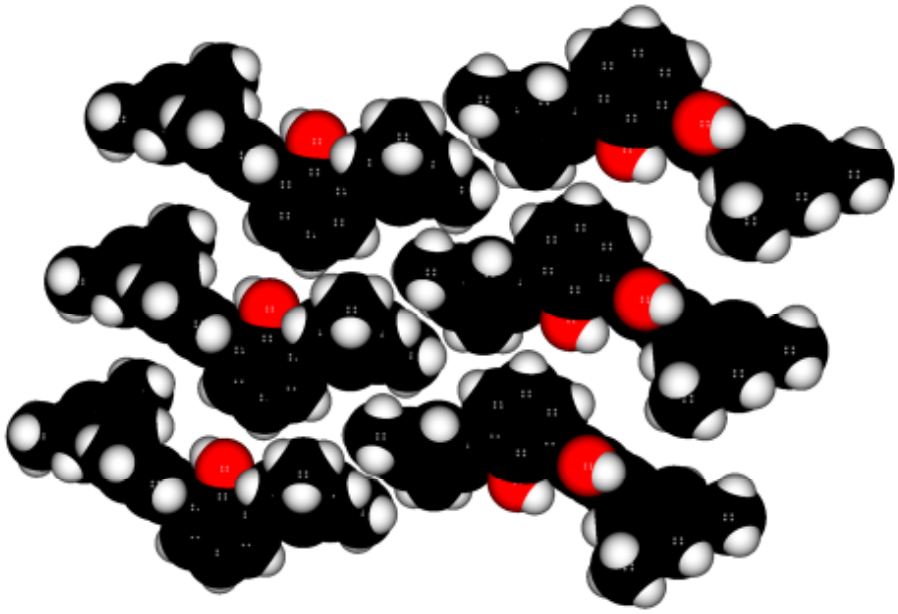

Figure 16: A 2D-layer of **http2** molecules stacked according to P-1 space-group symmetry.

The self-energy associated to the Pn stacking of **http2** molecules was found to be: SE_{net}(**http2**,Pn) = -621.3 kJ.mol^{-1}, leading to an average interaction energy: E_{int} = (2x309 – 621.3)/2 = -3.3/2 = -1.65 kJ.mol^{-1}. Figure 17 shows that this sub-net is made of chains of **http2** molecules at a distance of 300 pm. Again, there is a small stabilizing energy associated to this kind of stacking.

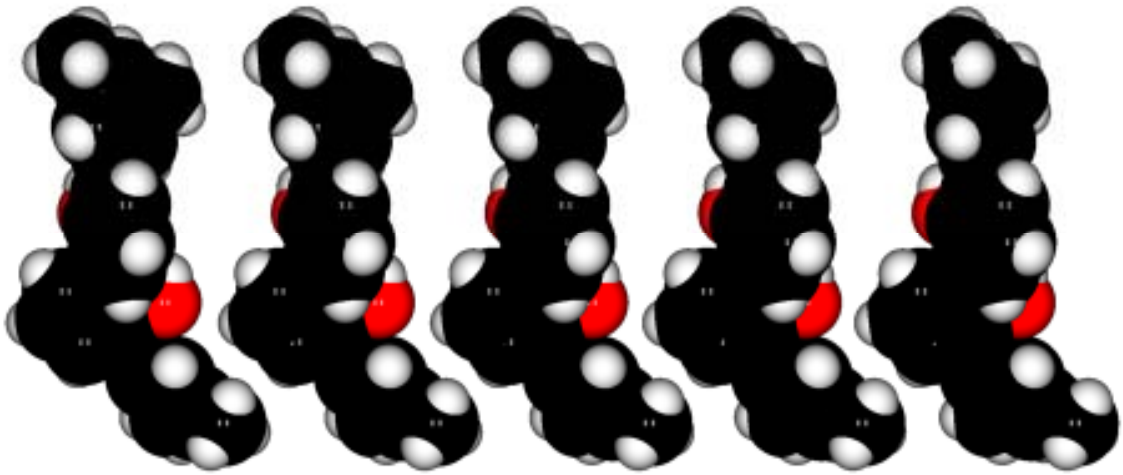

Figure 17: A 1D-chain of **http2** molecules stacked according to Pn space-group symmetry.

The average destabilization energy for the three isolated sub-nets ($P2_1$, P-1 and Pn) was –2.9 kJ.mol^{-1}, a value that should be compared to the –5.3 kJ.mol^{-1} value characterizing the three interacting sub-groups $P2_1/n$. This shows that there is a clear cooperative effect (2.9 – 5.3 = –2.4 kJ.mol^{-1}) among **http2** molecules again typical of van der Waals stacking.

Having characterized separated sub-nets of **http1** and **http2** molecules, we may then evaluate the effect of interweaving the two sub-nets. This leads to a global interaction energy E_{int} = [SE_{net}(**http1**) + SE_{net}(**http2**) - SE_{net}]/8 = (1309.2 + 1257.2 – 2658.4)/8 = -92/8 = -11.5 kJ.mol^{-1}. Comparing this value to the interaction energy involving isolated **http** molecules (-14.0 kJ.mol^{-1}), this shows again a clear cooperative effect (11.5 - 14.0) = -2.5 kJ.mol^{-1}. Here again, one may consider the three possible sub-groups. The self-energies associated to the ($P2_1$, P-1 and Pn) stacking of both **http1** and **http2** molecules were found to be very similar: SE_{net}(http,$P2_1$) = -1325.9 kJ.mol^{-1}, SE_{net}(http,P-1) = -1323.8 kJ.mol^{-1} and SE_{net}(http,Pn) = -1323.7 kJ.mol^{-1} (average value of –1324.5 kJ.mol^{-1}). The average interaction energy between http molecules is thus evaluated as E_{int} = (2x636.7 – 1324.5)/2 = -51.1/2 = -25.6 kJ.mol^{-1}. In order to get an idea of the importance of the van der Waals networking interactions relative to the intermolecular hydrogen, the self-energy of an isolated dimer was found to be SE(**http1**,**http2**,HB) = -655.8 kJ.mol^{-1}, leading to a molecular interaction energy E_{int} = (2x655.8 – 1324.5)/2 = -12.9/2 = -6.5 kJ.mol^{-1}. This demonstrates that the intermolecular (**http1**…**http2**) H-bonding is largely dominant (6.5 – 25.6 = 19.1 kJ.mol^{-1}) over the solid-state packing, even by considering the full space-group symmetry $P2_1/n$: E_{int} = (4x655.8 – 2658.4)/4 = -35.2/4 = -8.8 kJ.mol^{-1}.

Concerning the other intra-molecular H-bond existing within **http1** molecules, a different method for quantifying the associated H-bond energy has to be used, because the PACHA approach is not reliable when covalent bonds are broken. In this case, an alternative is to rotate the H-atom engaged into hydrogen bonding and follow how the self-energy or the steric energy change after a full rotation of 360°. Such a rotation allows generates an energy profile displaying minima and maxima whose energy differences give an idea of the associated H-bond energy. Figure 18 shows such an energy profile computed within an isolated **http1** molecule. There is a clear self-energy minimum for a (H2-O2-C16-C15) torsion angle of about –40° that compares rather well to the experimental torsion angle of about –30°. One may further notice that this minimum in electrostatic self-energy corresponds to a maximum of repulsive steric energy computed from assuming Gordon-Kim potentials. The energy differences between the maximum and the minimum of each curve are –41.6

kJ.mol^{-1} for the self-energy and of +2.0 kJ.mol^{-1} for the steric energy. An intra-molecular H-bond energy of about –40 kJ.mol^{-1} may thus be associated to this situation.

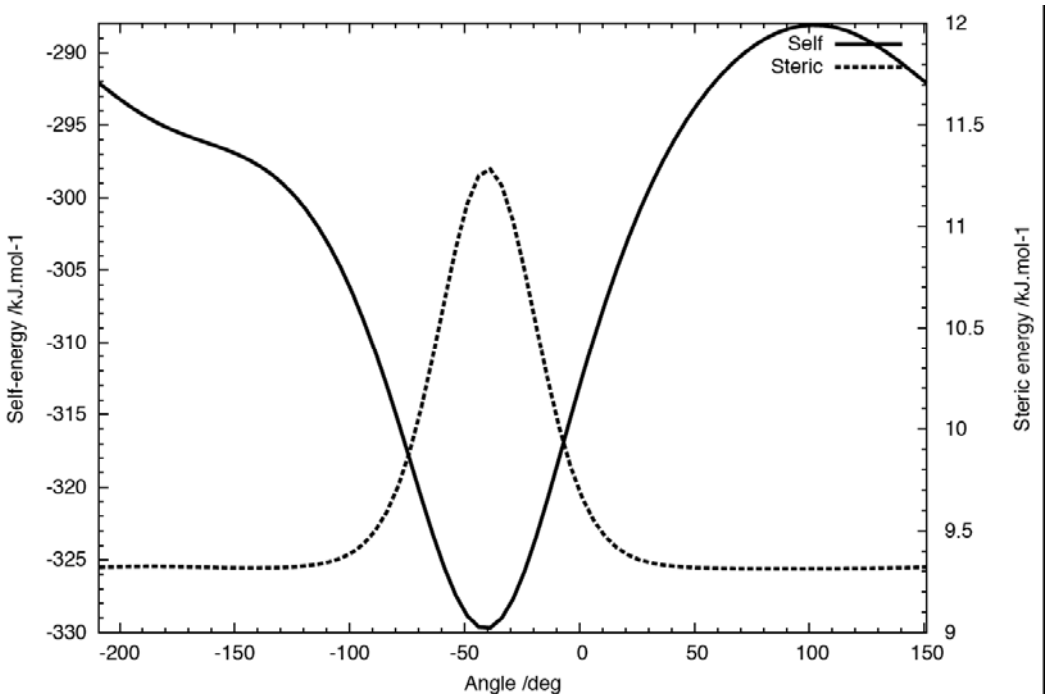

Figure 18: Energy profile obtained by rotating H2-atom by 360° within an isolated **http1** molecule.

In order to probe the importance of solid-state effect the same rotation was performed for the **http1** molecule embedded in its crystalline environment assuming full $P2_1/n$ space-group symmetry (figure 19). The second maximum in the steric energy curve is now due to the presence of an **http2** molecule H-bonded to **http1** while the self-energy minimum is obtained for a torsion angle of about –30° as observed experimentally. The energy differences are $\Delta E(self)$ = -213.0 kJ.mol^{-1} and $\Delta E(steric)$ = +7.8 kJ.mol^{-1} (Z = 4) leading to a H-bond energy of about (7.8 – 213.0)/4 = –50 kJ.mol^{-1}, a 20% increase relative to the isolated molecule.

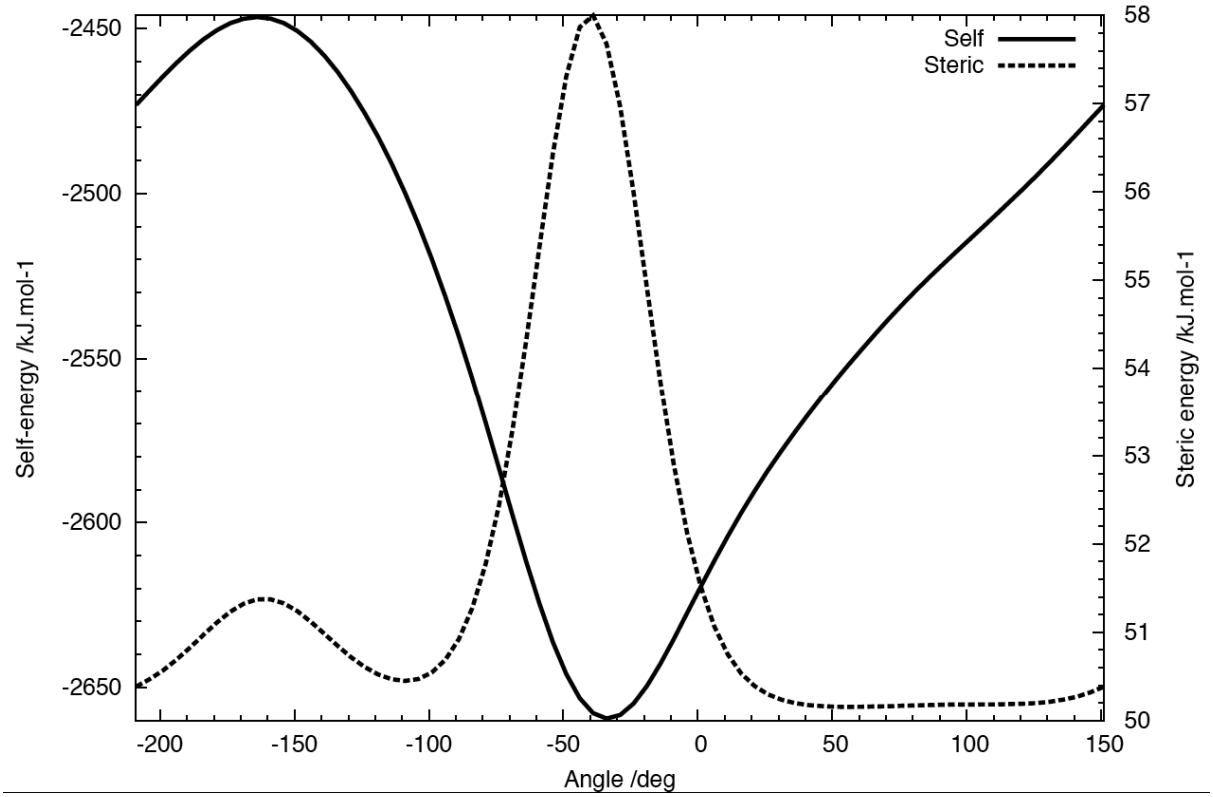

Figure 19: Energy profile obtained by rotating H2-atom by 360° for a **http1** molecule embedded into its crystalline environment.

Optimization of dichloromethane position in Phase I

As it was not possible to detect dichloromethane molecules embedded into the channels of **Phase I** and channels radii are large enough to accommodate such molecules, the most probable location of these molecules was investigated with PACHA. First a C-atom C29 was added at position (x,1/4,-1/8) and one chlorine atom Cl1 was added at 1.772 Å from C29 with two variable torsion angles (θ,φ). A second chlorine atom Cl2 was further added at 1.772 Å from C29 with a Cl1-C29-Cl2 bond angle of 112° and a variable torsion angle τ. Then two H-atoms H29 and H30 were added at 1.09 Å from the C-atom with H29-C29-Cl1 and H30-C29-H29 bond angles of 108.2° and 112° respectively and H29-C29-Cl1-Cl2 and H30-C29-H29-Cl1 torsion angles of 119.2°. These fixed bond lengths, bond angles and torsion angles were derived from the known structure of dichloromethane investigated after an ab-initio determination of the force field of this molecule verified by gas-phase infrared frequencies and intensities and combined electron diffraction and microwave study [30]. From this parameterization, the four independent variables (x, θ, φ, τ) were varied independently after minimization of the crystal self-energy. At convergence (SE = -1543.3 $kJ \cdot mol^{-1}$), the optimized coordinates for dichloromethane were found to be:

C29 (0,1/4,–1/8)

Cl1 (-0.00561,0.17266,0.93058)

Cl2 (-0.20435,0.25172,0.83710)

H29 (0.02175,0.31566,0.89261)

H30 (0.10445,0.23200,0.84521)

As shown in figure 20, these coordinates mean that chains of halogen-bonded dichloromethane molecules may be readily encapsulated within the channels of **Phase I**. The self-energy of such isolated chains being SE(chain) = -122.0 kJ·mol^{-1} (Z = 4) and that of a free dichloromethane molecule being SE(CH_2Cl_2) = -12.2 kJ·mol^{-1}, the halogen-bond energy may be estimated as: (12.2x4 – 122)/4 = -18.3 kJ·mol^{-1}. Similarly, the energy of encapsulation of such chains within the channels is found to be: (1319.7 + 122 – 1545.3)/4 = -103.6/4 = -25.9 kJ·mol^{-1}. The overall encapsulation energy of dichloromethane molecules within the network is thus 18.3 + 25.9 = 44.2 kJ·mol^{-1}.

Figure 20: Chains of dichloromethane molecule trapped within the channels of **Phase I** structure after self-energy minimization.

Optimization of pentane position in Phase I

As it was not possible to detect pentane molecules embedded into the channels of **Phase I** and channels radii are large enough to accommodate such molecules, the most probable location of these molecules was investigated with PACHA. First a C-atom C29 was added at position (x,1/4,-1/8) and one carbon atom C30 was added at 1.54 Å from C29 with two variable torsion angles (θ,φ). A third carbon atom C31 was further added at 1.54 Å from C30 with a C31-C30-C29 bond angle of 109.5° and a variable torsion angle τ_1. Similarly a fourth carbon atom C32 was added at 1.54 Å from the C31 with C32-C31-C30 bond angle of 109.5° and a variable torsion angle τ_2. Finally a fifth carbon atom C33 was added at 1.54 Å

from the C31 with C33-C32-C31 bond angle of 109.5° and a variable torsion angle τ_3. All these C-atoms were further protonated assuming C-H bond lengths of 1.08 Å, ideal tetrahedral bond and torsion angles. Two torsion angles τ_4 and τ_5 (one for each methyl-end) were assumed to be variable. From this parameterization, the eight independent variables (x, θ, φ, τ_1, τ_2, τ_3, τ_4, τ_5) were varied independently after minimization of the crystal steric energy using repulsive atom-atom potentials derived from the Gordon–Kim electron gas model, that have been tabulated for s and p elements up to Kr [31]. At convergence (SE = -1497.0 kJ·mol^{-1}), the optimized coordinates for pentane molecules were found to be:

C29 (0.06628,1/4,7/8)
C30 (0.08768,0.19387,0.92824)
C31 (0.25549,0.13486,0.92290)
C32 (0.25966,0.09222,0.86454)
C33 (0.36059,0.00335,0.86742)
H29 (0.09741,0.31827,0.88426)
H30 (0.15679,0.22585,0.84324)
H31 (-0.07037,0.24524,0.86017)
H32 (0.10232,0.23703,0.96389)
H33 (0.02965,0.15272,0.93369)
H34 (0.37458,0.17464,0.92871)
H35 (0.25122,0.08360,0.95429)
H36 (0.12391,0.08093,0.85034)
H37 (0.32755,0.13593,0.83578)
H38 (0.32543,-0.03661,0.83167)
H39 (0.50356,0.01545,0.86741)
H40 (0.32356,-0.03113,0.90519)

Figure 21 shows the predicted conformation for the pentane molecules encapsulated within the channels of **Phase I** while figure 22 shows the predicted packing geometry. The self-energy of such isolated chains being SE(chain) = -172.9 kJ·mol^{-1} (Z = 4) and that of a free pentane molecule being SE(C_5H_{12}) = -42.9 kJ·mol^{-1}, the interaction energy may be estimated as: (42.9x4 – 172.9)/4 = -1.3/4 = -0.3 kJ·mol^{-1}. Similarly, the energy of encapsulation of such chains within the channels is found to be: (1319.7 + 172.9 – 1497.0)/4

= -4.4/4 = -1.1 kJ·mol^{-1}. The overall encapsulation energy of pentane molecules within the network is thus -(1.1 + 0.3) = -1.4 kJ·mol^{-1}.

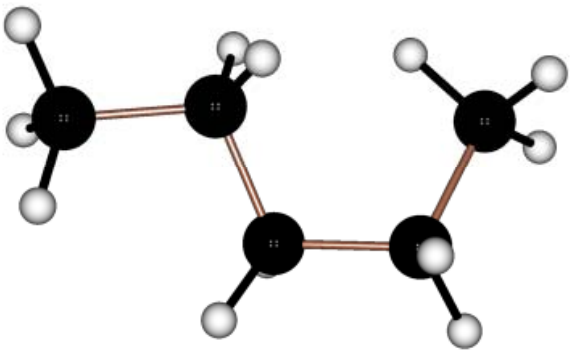

Figure 21: Equilibrium conformation for pentane molecules trapped within the channels of **Phase I** structure after steric energy minimization.

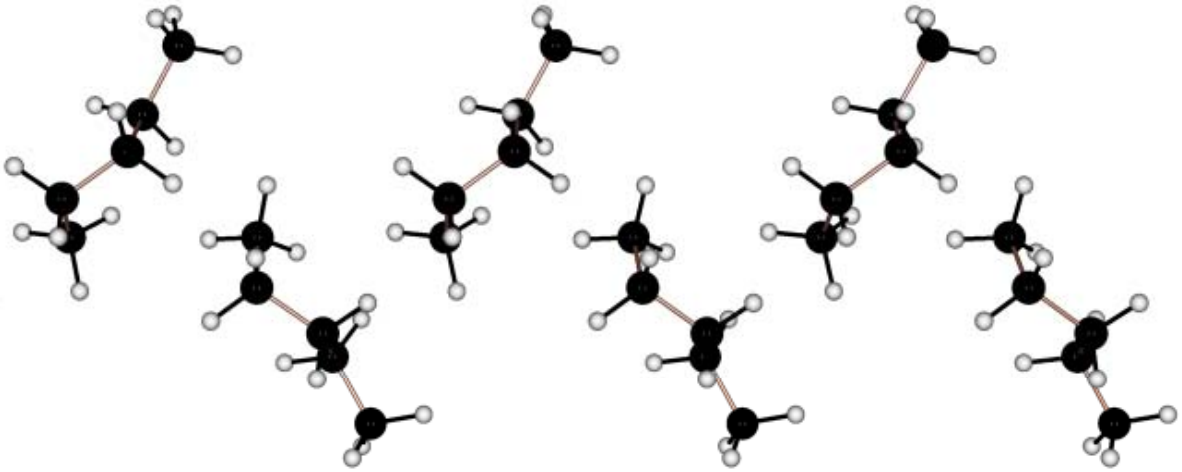

Figure 22: Predicted packing geometry for pentane molecules trapped within the channels of **Phase I** structure after steric energy minimization.

Optimization of pentane and dichloromethane position in Phase I

Finally the possibility of having both dichloromethane and pentane molecules in the channels was investigated with PACHA. First a C-atom C29 was added at position (x_1,y_1,z_1) and one carbon atom C30 was added at 1.54 Å from C29 with two variable torsion angles (θ_1,φ_1). A third carbon atom C31 was further added at 1.54 Å from C30 with a C31-C30-C29 bond angle of 109.5° and a variable torsion angle τ_1. Similarly a fourth carbon atom C32 was

added at 1.54 Å from the C31 with C32-C31-C30 bond angle of 109.5° and a variable torsion angle τ_2. Finally a fifth carbon atom C33 was added at 1.54 Å from the C31 with C33-C32-C31 bond angle of 109.5° and a variable torsion angle τ_3. All these C-atoms were further protonated assuming C-H bond lengths of 1.08 Å, ideal tetrahedral bond and torsion angles. Two torsion angles τ_4 and τ_5 (one for each methyl-end) were assumed to be variable. For dichloromethane, a C-atom C34 was added at position (x_2,y_2,z_2) and one chlorine atom Cl1 was added at 1.772 Å from C29 with two variable torsion angles (θ_2,φ_2). A second chlorine atom Cl2 was further added at 1.772 Å from C34 with a Cl1-C29-Cl2 bond angle of 112° and a variable torsion angle τ_6. Then two H-atoms H60 and H61 were added at 1.09 Å from the C-atom with H29-C29-Cl1 and H30-C29-H29 bond angles of 108.2° and 112° respectively and H29-C29-Cl1-Cl2 and H30-C29-H29-Cl1 torsion angles of 119.2° and –121.6 respectively. These fixed bond lengths, bond angles and torsion angles were derived from the known structure of dichloromethane investigated after an ab-initio determination of the force field of this molecule verified by gas-phase Infrared frequencies and intensities and combined electron diffraction and microwave study [30]. From this parameterization, the 16 variables (x_1, y_1, z_1, θ_1, φ_1, τ_1, τ_2, τ_3, τ_4, τ_5, x_2, y_2, z_2, θ_2, φ_2, τ_6) were varied independently after minimization of the crystal steric energy using repulsive atom-atom potentials derived from the Gordon–Kim electron gas model, that have been tabulated for s and p elements up to Kr [31]. At convergence (SE = -1709.5 $kJ \cdot mol^{-1}$), the optimized coordinates for pentane and dichloromethane molecules were found to be:

C29 0.12407 0.02476 0.84889
C30 0.25988 0.01112 0.89660
C31 0.41334 0.07891 0.89103
C32 0.48365 0.10350 0.94945
C33 0.63962 0.04144 0.96531
H29 -0.01075 0.02282 0.86548
H30 0.14752 0.08820 0.82942
H31 0.14021 -0.02717 0.81832
H32 0.19314 0.02019 0.93621
H33 0.31427 -0.05507 0.89437
H34 0.52109 0.05048 0.86675
H35 0.36395 0.13766 0.87043

H36 0.53063 0.17115 0.94921

H37 0.37661 0.09664 0.97956

H38 0.74847 0.07988 0.98264

H39 0.59381 -0.00603 0.99586

H40 0.68596 0.00694 0.92855

C34 0.32984 0.31247 0.80615

Cl1 0.15173 0.36581 0.77043

Cl2 0.32499 0.33430 0.87879

H60 0.31581 0.24129 0.80008

H61 0.45874 0.33694 0.79107

Figure 23 shows the predicted conformation for the pentane molecules encapsulated within the channels of **Phase I** while figure 22 shows the predicted packing geometry of both kind of molecules. The self-energy of such isolated chains of solvent molecules being SE(chain) = -347.7 kJ·mol^{-1} (Z = 4) and that of a free pentane molecule and a free dichloromethane molecule being SE(C_5H_{12}) = -43.0 kJ·mol^{-1} and SE(CH_2Cl_2) = -12.2 kJ·mol^{-1} respectively, the interaction energy may be estimated as: (42.9x4 + 12.2x4 – 347.7)/4 = -127.3/4 = -31.8 kJ·mol^{-1}.

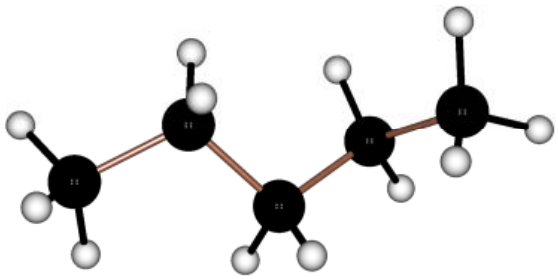

Figure 23: Equilibrium conformation for pentane molecules trapped with dichloromethane molecules within the channels of **Phase I** structure after steric energy minimization.

Similarly, the energy of encapsulation of such chains within the channels is found to be: (1319.7 + 347.7 – 1709.5)/4 = -42.1/4 = -10.5 kJ·mol^{-1}. The overall encapsulation energy of solvent molecules within the network is thus -(31.8 + 10.5) = -42.3 kJ·mol^{-1}.

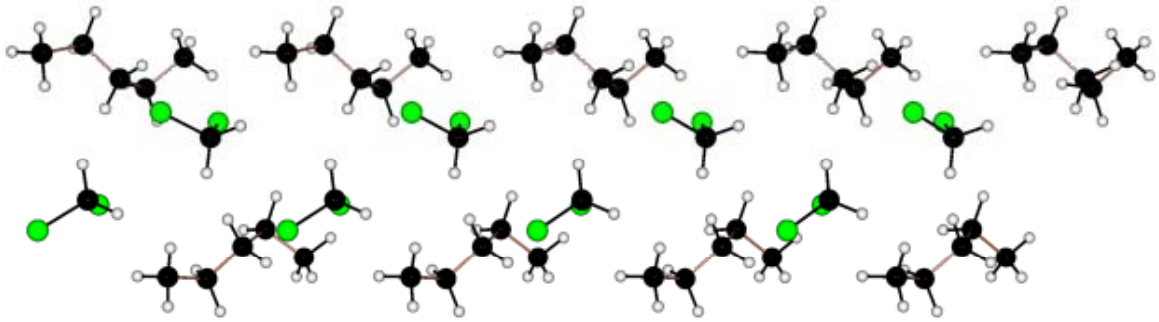

Figure 24: Predicted packing geometry for pentane and dichloromethane molecules trapped within the channels of **Phase I** structure after steric energy minimization.

One may also investigate the interaction of dichloromethane molecules with the network partially filled with pentane molecules as $SE_{net}(pent)$ = -1498.5 kJ·mol^{-1} and $SE_{chain}(CH_2Cl_2)$ = -53.6 kJ·mol^{-1} leading to (1495.8 + 53.6 – 1709.5)/4 = -160.1/4 = -40.0 kJ·mol^{-1}. Concerning the interaction of pentane molecules with the network partially filled with dichloromethane molecules we got $SE_{net}(CH_2Cl_2)$ = -1483.0 kJ·mol^{-1} and $SE_{chain}(pent)$ = -171.7 kJ·mol^{-1} leading to (1483.0 + 171.7 – 1709.5)/4 = -54.8/4 = -13.7 kJ·mol^{-1}.

[1] M. Henry, *CHEMPHYSCHEM*, 2002, **3**, 561.

[2] M. Henry, in: Mihai V. Putz (Ed), *Advances in Quantum Chemical Bonding Structures*, Transworld Research Network: Kerala, India, 2008, 153-211.

[3] M. Henry, *J. Cluster Sci.* 2002, **13**, 437.

[4] M. Henry, *CHEMPHYSCHEM*, 2002, **3** , 607.

[5] L. Beitone, J. Marrot, T. Loiseau, G. Férey, M. Henry, C. Huguenard, A. Gansmuller and F. Taulelle *J. Am. Chem. Soc.* 2003, **125**, 1912.

[6] J.M. Douillard & M. Henry, *J. Colloid Interface Sci.* 2003, **263**, 554.

[7] L. Beitone, C. Huguenard, A. Gansmuller, M. Henry, F. Taulelle, T. Loiseau & G. Férey, *J. Am. Chem. Soc.* 2003, **125**, 9102.

[8] M. Henry, *Solid State Sciences*, 2003, **5**, 1201.

[9] A. Müller and M. Henry, *C. R. Chimie*, 2003, **6**, 1201.

[10] M. Henry, *J. Cluster Sci.* 2003, **14**, 267.

[11] T. Loiseau, C. Serre, C. Huguenard, G. Fink, F. Taulelle, M. Henry, T. Bataille and G. Férey *Chem. Eur. J.* 2004, **10**, 1373.

[12] M. Henry, F. Taulelle, T. Loiseau, L. Beitone and G. Férey, *Chem. Eur. J.* 2004, **10**, 1366.

[13] F. Biechel, J. Dubuc and M. Henry, *New J. Chem.* 2004, **28**, 764.

[14] M. Henry and M. W. Hosseini, *New J. Chem.* 2004, **28**, 897.

[15] A. Senouci, M. Yaakoub, C. Huguenard and M. Henry, *J. Mater. Chem.* 2004, **14**, 3215.

[16] A. Müller, H. Bögge and M. Henry, *C. R. Chimie*, 2005, **8**, 47.

[17] M. Henry, H. Bögge, E. Diemann and A. Müller, *J. Molecular Liquids*, 2005, **118**, 155.

[18]Turner, D.R., Henry, M., Wilkinson, C., McIntyre, G.J., Mason, S.A., Goeta, A.E. and J.W. Steed, *J. Am. Chem. Soc.* 2005, **127**, 11063.

[19] G.I. Spijsma, H.J.M. Bouwmeester, D.H.A. Blank, A. Fischer, M. Henry and V.G. Kessler, *Inorg. Chem.* 2006, **45**, 4938.

[20] A. Müller, L. Toma, H. Bögge, M. Henry, E. T. K. Haupt, A. Mixa and F. L. Sousa, *Chem. Commun.* 2006, 3396.

[21] F. Salles, M. Henry and J.M. Douillard, *J. Coll. Interface. Sci.* 2006, **303**, 617.

[22] J.M. Douillard, F. Salles, S. Devautour-Vinot, A. Manteghetti and M. Henry, *J. Coll. Interface. Sci.*, 2007, **306**, 175.

[23] J.M. Douillard, F. Salles, M. Henry, H. Malandrini and F. Clauss, *J. Coll. Interface. Sci.* 2007, **307**, 352.

[24] A. Haouzi, E. Salles, M. Henry and J.M. Douillard, *J. Coll. Interface. Sci.* 2007, **307**, 531.

[25] A.M. Todea, A. Merca, H. Bögge, J. van Slageren, M. Dressel, L. Engelhardt, M. Luban, T. Glaser, M. Henry and A. Müller, *Angew. Chem. Int. Ed.* 2007, **4**, 6106.

[26] J.-F. Lemonnier, S. Floquet, J. Marrot, A. Kachmar, M. Bénard,‡ M.-M. Rohmer, M. Haouas, F. Taulelle, M. Henry and E. Cadot, *Inorg. Chem.* 2007, **46**, 9516-9518.

[27] J.M. Douillard, S. Lantenois, B. Prelot, J. Zajac and M. Henry, *J. Colloid Interface Sci.* 2008, **325**, 275.

[28] C. Carpanese, S. Ferlay, N. Kyritsakas, M. Henry and M.W. Hosseini, *Chem. Comm.* 2009, 6786.

[29] H. Senouci, B. Millet, C. Volkringer, C. Huguenard, F. Taulelle and M. Henry, *C. R. Chimie*, 2010, **13**, 69.

[30] Y. Wang, J. Tremmel, J. De Smedt, C. Van Alseny, H.J. Geise and B. Van der Veken, *J. Phys. Chem. A*, 1997, **101**, 5919.

[31] M. A. Spackman, *J. Chem. Phys.* 1986, **85**, 6579.